JACS
JOURNAL OF THE AMERICAN CHEMICAL SOCIETY
Article
pubs.acs.org/JACS

Heavy Doping and Band Engineering by Potassium to Improve the Thermoelectric Figure of Merit in p-Type PbTe, PbSe, and $PbTe_{1-y}Se_y$

Qian Zhang,[†] Feng Cao,[†] Weishu Liu,[†] Kevin Lukas,[†] Bo Yu,[†] Shuo Chen,[†] Cyril Opeil,[†] David Broido,[†] Gang Chen,*[,‡] and Zhifeng Ren*[,†]

[†]Department of Physics, Boston College, Chestnut Hill, Massachusetts 02467, United States
[‡]Department of Mechanical Engineering, Massachusetts Institute of Technology, Cambridge, Massachusetts 02139, United States

Supporting Information

ABSTRACT: We present detailed studies of potassium doping in $PbTe_{1-y}Se_y$ (y = 0, 0.15, 0.25, 0.75, 0.85, 0.95, and 1). It was found that Se increases the doping concentration of K in PbTe as a result of the balance of electronegativity and also lowers the lattice thermal conductivity because of the increased number of point defects. Tuning the composition and carrier concentration to increase the density of states around the Fermi level results in higher Seebeck coefficients for the two valence bands of $PbTe_{1-y}Se_y$. Peak thermoelectric figure of merit (ZT) values of ~1.6 and ~1.7 were obtained for Te-rich $K_{0.02}Pb_{0.98}Te_{0.75}Se_{0.25}$ at 773 K and Se-rich $K_{0.02}Pb_{0.98}Te_{0.15}Se_{0.85}$ at 873 K, respectively. However, the average ZT was higher in Te-rich compositions than in Se-rich compositions, with the best found in $K_{0.02}Pb_{0.98}Te_{0.75}Se_{0.25}$. Such a result is due to the improved electron transport afforded by heavy K doping with the assistance of Se.

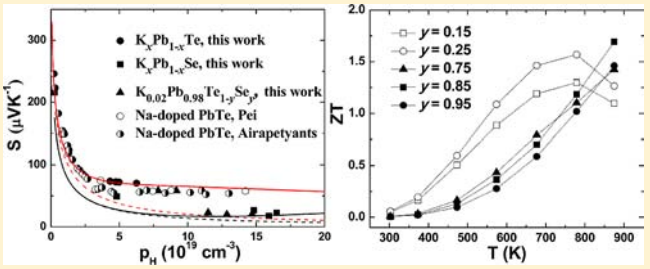

INTRODUCTION

Intensive attention has recently been paid to energy conversion using thermoelectric principles, which can directly convert both waste heat and solar energy into electricity.[1−3] Large-scale applications call for thermoelectric materials with high values of the dimensionless figure of merit $ZT = [S^2\sigma/(\kappa_L + \kappa_e)]T$, where S is the Seebeck coefficient, σ is the electrical conductivity, κ_L is the lattice thermal conductivity, κ_e is the charge-carrier thermal conductivity, and T is the absolute temperature.[4−7] Accordingly, a combination of a high Seebeck coefficient with high electrical conductivity and low thermal conductivity is desired and has been pursued. However, it is difficult to optimize one parameter without deteriorating the others. Complex crystals are normally considered to have the advantage of decoupling the three interrelated quantities with the concept of "electron−crystal phonon−glass".[8−10] Nanostructuring is the major approach for ZT enhancement, since it allows independent tuning of all of the parameters.[11−17]

Lead telluride (PbTe) with the simple face-centered-cubic (fcc) rock salt structure is one of the most studied thermoelectric materials suitable for the intermediate temperature range (600−800 K).[18−21] Its cheaper sister compound lead selenide (PbSe) also has a decent value of ZT.[22−24] Excellent progress has recently been made through band engineering, such as resonant states[18,19,23] and band convergence,[20,22,25,26] leading to improvements in both the electrical conductivity and Seebeck coefficient simultaneously without affecting the thermal conductivity too much.[27] Good results were reported for Tl-doped PbTe, which pushed the ZT value to ~1.5 at 773 K by creating resonant states near the Fermi energy.[18] Recently, Al doping was reported to result in n-type resonant doping in PbSe with a peak ZT value of ~1.3.[23] A great deal of theoretical work has been performed to find possible new resonant dopants in PbTe and PbSe.[28−30] It was predicted that the alkali metals K, Rb, and Cs can create resonant density of states (DOSs) distortion in PbTe, whereas Na cannot because it does not change the DOS near the top of the valence band.[28] However, PbTe doped heavily with Na still exhibits high ZT values, which are believed to be the result of the coexistence of light-hole (L) and heavy-hole (Σ) valence bands in PbTe.[31] Effective doping of Na moves the Fermi level close to the Σ band, which has a much larger DOS, helping increase the Seebeck coefficient.[20,32−34] A ZT value of ~1.4 at 750 K in Na-doped PbTe with a Hall carrier concentration (p_H) greater than $\sim 7.5 \times 10^{19}$ cm^{-3} has been obtained.[20] A similar effect has been shown theoretically and experimentally in PbSe, which has a flat, high-mass, high-DOS band 0.35−0.4 eV below the valence-band maximum.[35] ZT values reaching 1.2−1.3 at 850 K have been reported for Na-doped PbSe with a Hall carrier concentration of $(9-15) \times 10^{19}$ cm^{-3}.[22] Furthermore, a ZT value of ~1.8 at ~850 K was reported for $Na_{0.02}Pb_{0.98}Te_{0.85}Se_{0.15}$ as a result of alloying with Se.[25] Regardless of whether the increase in the electronic power factor (σS^2) is due to resonant levels or the Σ band, it is obvious that band engineering can enhance the carrier (electron/hole) transport. Indeed, both resonant states and band convergence contribute to the high ZT value in Tl-doped

Received: February 7, 2012
Published: May 24, 2012

Table 1. Theoretical Densities (D_T), Measured Volumetric Densities (D), Relative Densities (D_R), and Electrical Conductivity Power Law Exponents (δ) for $K_xPb_{1-x}Te$, $K_xPb_{1-x}Se$, and $K_{0.02}Pb_{0.98}Te_{1-y}Se_y$

	$K_xPb_{1-x}Te$				$K_xPb_{1-x}Se$			$K_{0.02}Pb_{0.98}Te_{1-y}Se_y$				
	0.01	0.0125	0.015	0.02	0.01	0.0125	0.015	0.15	0.25	0.75	0.85	0.95
D_T (gcm^{-3})	8.18	8.18	8.17	8.14	8.19	8.18	8.18	8.09	8.10	8.13	8.13	8.14
D ($g\ cm^{-3}$)	8.06	8.02	8.02	8.01	7.84	7.9	7.92	7.97	7.99	7.97	7.91	8.02
D_R	99%	98%	98%	98%	96%	97%	97%	99%	99%	98%	97%	99%
δ	3.11	2.95	3	2.94	3.17	2.8	2.99	2.34	2.4	2.58	2.9	2.87

PbTe.[26] However, it is desired to avoid Tl for practical applications because of its toxicity. Motivated by recent calculations,[28] we chose to study K doping to make $K_xPb_{1-x}Te_{1-y}Se_y$ because of the smaller ionic radius of K^+ compared with Rb^+ and Cs^+. Normally, it is believed that K has a limited solubility in PbTe,[26,36] which limits the Hall carrier concentration to less than 6×10^{19} cm^{-3}. Thus, reports on K doping in PbTe have been very limited, in contrast to Na doping in PbTe, which can produce much higher carrier concentrations. In this work, we were able to increase the Hall carrier concentration to $(8-15) \times 10^{19}$ cm^{-3} in PbTe by K doping with the help of Se through the balance of electronegativity. It is shown that band engineering works well in $K_xPb_{1-x}Te_{1-y}Se_y$, giving a higher Seebeck coefficient. Peak ZT values of ~1.6 and ~1.7 were obtained in Te-rich $K_{0.02}Pb_{0.98}Te_{0.75}Se_{0.25}$ and Se-rich $K_{0.02}Pb_{0.98}Te_{0.15}Se_{0.85}$, respectively. However the average ZT of the Te-rich compositions was higher, making this material more favorable for practical applications.

EXPERIMENTAL SECTION

Synthesis. Ingots with nominal compositions $K_xPb_{1-x}Te$ (x = 0.01, 0.0125, 0.015, and 0.02), $K_xPb_{1-x}Se$ (x = 0, 0.005, 0.01, 0.0125, and 0.025), and $K_{0.02}Pb_{0.98}Te_{1-y}Se_y$ (y = 0.15, 0.25, 0.75, 0.85, and 0.95; other compositions such as y = 0.4 and 0.5 were also studied, but those results have not been shown here to increase the readability of the figures) were prepared in a quartz tube with carbon coating. The raw materials inside the quartz tube were slowly raised to 1000−1100 °C and kept there for 6 h, then slowly cooled to 650 °C and maintained at that temperature for 50 h, and finally slowly cooled to room temperature. The obtained ingots were cleaned and hand-milled in a glovebox. The sieved (325 mesh) powder was loaded into a half-inch die and hot-pressed at 500−600 °C for 2 min. The hot-pressed pellets were sealed in a quartz tube for further annealing at 600 °C for 4 h to make the sample stable during the measurements at temperatures up to 600 °C.

Characterizations. X-ray diffraction (XRD) analysis was conducted on a PANalytical multipurpose diffractometer with an X'celerator detector (PANalytical X'Pert Pro). The electrical resistivity (ρ) and the Seebeck coefficient were measured using a four-point direct-current switching method and the static temperature difference method, respectively, both of which were conducted on a commercial system (ULVAC ZEM-3). The thermal diffusivity (α) was measured on a laser flash apparatus (Netzsch LFA 447), and the specific heat (C_p) was measured on a differential scanning calorimetry thermal analyzer (Netzsch DSC200-F3). The volumetric density (D) was measured by the Archimedes method and is shown in Table 1 along with the theoretical density (D_T). The thermal conductivity (κ) was calculated as $\kappa = D\alpha C_p$. The Hall coefficient (R_H) at room temperature was measured using a Quantum Design Physical Properties Measurement System. The Hall carrier concentration (n_H) and Hall mobility (μ_H) were calculated as $n_H = (eR_H)^{-1}$ and $\mu_H = \sigma R_H$. It is understood that there is a 3% error in the electrical conductivity, 5% error in the Seebeck coefficient, and 4% error in the thermal conductivity, resulting in errors of 10% for the power factor and 11% for ZT. For better readability of the figures, we have deliberately plotted the curves without the error bars.

RESULTS AND DISCUSSION

On the basis of the ionic radii of Pb, Na, and K (Table 2), K^+ is closer to Pb^{2+} but a little bigger. For samples $K_xPb_{1-x}Te$ (x = 0.01, 0.0125, 0.015, and 0.02), the electrical conductivity, Seebeck coefficient, power factor, thermal diffusivity, specific heat, lattice thermal conductivity, and total thermal conductivity were measured, and the results are presented in Figure 1a−f, respectively. The electrical conductivity at room temperature increased a little bit with increasing K concentration, but no change was seen at high temperature, where all of the samples showed a decrease with temperature (Figure 1a). The Seebeck coefficients of all of the samples (Figure 1b) changed only slightly, likely as a result of contributions from both the light and heavy holes with the high carrier concentration.[26] The power factor increased with increasing K concentration and peaked at ~500 K (Figure 1c). The thermal diffusivity was basically the same for all of the samples (Figure 1d), consistent with the microstructures (see the Supporting Information). The specific heats of the samples were similar (Figure 1e), indicating good repeatability of the measurements. Combining the thermal diffusivities, specific heats, and volumetric densities gave the thermal conductivities (Figure 1f), which were very close to each other.

Table 2. Ionic Radii (r) and Pauling Electronegativities (PE) of K, Na, Pb, Te, and Se

	K	Na	Pb	Te	Se
r (Å)	1.33	0.97	1.20	2.11	1.91
PE	0.82	0.93	2.33	2.10	2.55

To provide a better understanding of the band structure of $K_xPb_{1-x}Te$, a Pisarenko plot (Seebeck coefficient vs Hall carrier concentration) at room temperature was made (Figure 2, solid circles) and compared with reported results for Na-doped PbTe (open and half-open circles).[20,32] The Hall carrier concentration of our K-doped PbTe samples (<6.3×10^{19} cm^{-3}) was lower than that in Na-doped PbTe, which could be as high as 14×10^{19} cm^{-3}. The flattening of the Seebeck coefficient with increasing carrier concentration indicates a contribution from the second valence band. This behavior has been explained previously using a multiband model with a nonparabolic L band described by a Kane model and a parabolic Σ band,[25,26,37] and we employed a similar model here.

The Seebeck coefficient S_L and carrier concentration p_L for a single nonparabolic light-hole band at the L point are given by

$$S_L = \pm\frac{k_B}{e}\left[\frac{{}^1F^1_{-2}(\eta,\beta)}{{}^0F^1_{-2}(\eta,\beta)} - \eta\right] \quad (1)$$

dx.doi.org/10.1021/ja301245b | J. Am. Chem. Soc. 2012, 134, 10031−10038

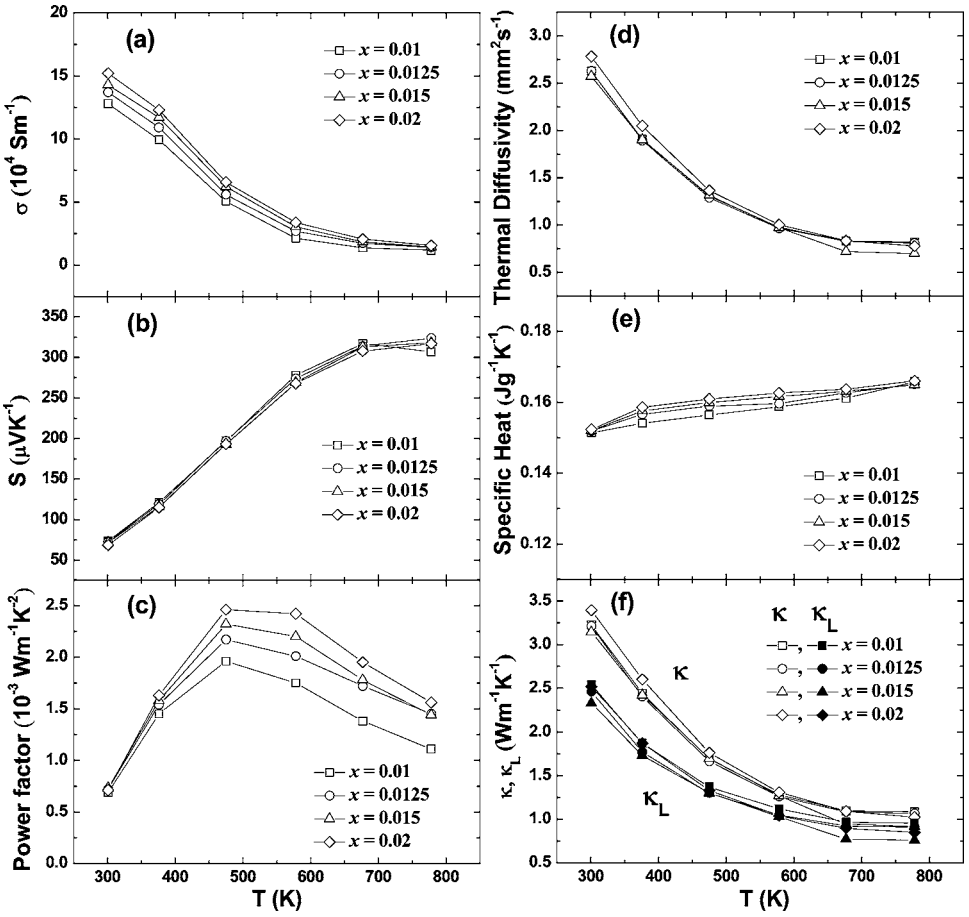

Figure 1. Temperature dependences of (a) electrical conductivity, (b) Seebeck coefficient, (c) power factor, (d) thermal diffusivity, (e) specific heat, and (f) total and lattice thermal conductivities for $K_xPb_{1-x}Te$ (x = 0.01, 0.0125, 0.015, and 0.02).

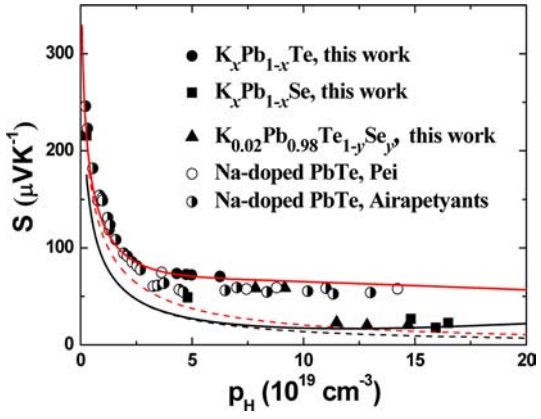

Figure 2. Room-temperature Pisarenko plots for (●) $K_xPb_{1-x}Te$ (x = 0.01, 0.0125, 0.015, and 0.02), (■) $K_xPb_{1-x}Se$ (x = 0, 0.005, 0.010, 0.0125, and 0.015), and (▲) $K_{0.02}Pb_{0.98}Te_{1-y}Se_y$ (y = 0.15, 0.25, 0.75, 0.85, and 0.95). For comparison, data for Na-doped PbTe reported by (○) Pei et al.[20] and (◑) Airapetyants et al.[32] are also shown. The dashed black curve is based on a model employing a single nonparabolic band with a PbSe light-hole effective mass of m^*/m_e = 0.28. The solid black curve is based on a two-band model (nonparabolic L band and parabolic Σ band) with a PbSe heavy-hole effective mass of m^*/m_e = 2.5. The dashed red curve is based on a model employing a single nonparabolic band with a PbTe light-hole effective mass of m^*/m_e = 0.36. The solid red curve is based on a two-band model (nonparabolic L band and parabolic Σ band) with a PbTe heavy-hole effective mass of m^*/m_e = 2.

$$p_L = \frac{1}{3\pi^2}\left(\frac{2m_L^* k_B T}{h^2}\right)^{3/2} {}^0F_0^{3/2}(\eta, \beta) \quad (2)$$

where k_B is Boltzmann's constant, e is the electron charge, ${}^nF_k^m$ is the generalized Fermi function,[37] η is the reduced Fermi level, h is Planck's constant, and m_L^* is the light-hole DOS effective mass, taken as m_L^*/m_e = 0.36.[37] The nonparabolicity parameter, β, is given by $\beta = k_BT/E_g$, where E_g is the L-point band gap. We assumed that deformation potential scattering by acoustic phonons dominates.[20,25,37] We also did the calculation including ionized impurity scattering for the nonparabolic L band. The relaxation time for ionized impurities, τ_I, is much larger than that for deformation potential scattering, τ_D. When the relaxation times were combined using Matheiessen's rule ($1/\tau = 1/\tau_I + 1/\tau_D$), there was almost no difference in S_L relative to the result when only τ_D was included. For the heavy-hole band, taken along the Σ direction in the Brillouin zone,[37] the Seebeck coefficient S_Σ and carrier concentration p_Σ are given by

$$S_\Sigma = \frac{k_B}{e}\left[\frac{{}^1F_{-2}^1(\eta_\Sigma, 0)}{{}^0F_{-2}^1(\eta_\Sigma, 0)} - \eta_\Sigma\right] \quad (3)$$

$$p_\Sigma = \frac{1}{3\pi^2}\left(\frac{2m_\Sigma^* k_B T}{h^2}\right)^{3/2} {}^0F_0^{3/2}(\eta_\Sigma, 0) \quad (4)$$

dx.doi.org/10.1021/ja301245b | J. Am. Chem. Soc. 2012, 134, 10031−10038

where m_Σ^* is the heavy-hole DOS effective mass, taken as $m_\Sigma^*/m_e = 2$,[38] and $\eta_\Sigma = \eta - \Delta E/k_BT$, where ΔE is the energy difference between the light-hole and heavy-hole band maxima, whose value is discussed below. It should be noted that for this parabolic band, $\beta = 0$. The total Seebeck coefficient from both hole bands, S_{total}, is taken to be:

$$S_{total} = \frac{\sigma_L S_L + \sigma_\Sigma S_\Sigma}{\sigma_L + \sigma_\Sigma} \quad (5)$$

where σ_L and σ_Σ are the electrical conductivities of the L and Σ bands, respectively.[37]

The total Hall carrier concentration for a two-band system, p_H, is related to the carrier concentrations in the two bands, p_L and p_Σ, as described previously in refs 25 and 37 (this expression is provided in the Supporting Information and in refs 25 and 37). In Figure 2, the solid red line shows the calculated S_{total} as a function of p_H for PbTe. It can be seen that the data (solid circles) falls nicely on the flat part of the solid red line at $S \approx 75\ \mu V\ K^{-1}$, indicating a clear contribution from two bands as a result of K doping. Alternatively, Kanatzidis et al.[26] obtained a plateau at $S \approx 56\ \mu V\ K^{-1}$ using a light-hole effective mass of $\sim 0.2m_e$, which can explain Na-doped PbTe pretty well. The magnitude of the heavy-hole contribution was highlighted by examining a one-band light-hole model obtained by removing the contribution from the Σ band. This case gave the dashed red line shown in Figure 2, which falls well below the measured data at high carrier concentrations.

As the temperature increased, the Seebeck coefficient increased dramatically to $\sim 320\ \mu V\ K^{-1}$ at 775 K, a value much higher even than that for Na-doped PbTe ($\sim 260\ \mu V\ K^{-1}$ at 775 K), which is believed to be due to the two-band contribution.[20] In view of the fact that first-principles calculations predicted possible resonant states introduced by K doping,[28] it is likely that resonant doping may also play a minor role here in addition to the two-band contribution. However, we do not have enough evidence to support this because the Seebeck coefficient is not high enough. The limited carrier concentration of $< 6 \times 10^{19}\ cm^{-3}$ resulting from K doping restrains the increase in the electrical conductivity (shown in Figure 1 a), which is the determining factor when the S flattens. Furthermore, the decrease in electrical conductivity with temperature is faster in K-doped samples, as exhibited by the values of δ, the exponents in the power law for the electrical conductivity ($\sigma \approx T^{-\delta}$), presented in Table 1.

Generally speaking, the total thermal conductivity κ is the sum of the charge-carrier thermal conductivity κ_e and the lattice thermal conductivity κ_L. The value of κ_e can be calculated via the Wiedemann–Franz relation, $\kappa_e = L\sigma T$, in which the Lorenz number L is the same for the electrons and holes; κ_L is then derived by subtracting κ_e from κ. Values of κ and κ_L are presented in Figure 1f. Again, a multiband model was employed for the accurate estimation of L. This model gives the following expressions:[37]

$$L_L = \left(\frac{k_B}{e}\right)^2 \left\{ \frac{{}^2F_{-2}^1(\eta, \beta)}{{}^0F_{-2}^1(\eta, \beta)} - \left[\frac{{}^1F_{-2}^1(\eta, \beta)}{{}^0F_{-2}^1(\eta, \beta)}\right]^2 \right\} \quad (6)$$

$$L_\Sigma = \left(\frac{k_B}{e}\right)^2 \left\{ \frac{{}^2F_{-2}^1(\eta_\Sigma, 0)}{{}^0F_{-2}^1(\eta_\Sigma, 0)} - \frac{{}^1F_{-2}^1(\eta_\Sigma, 0)}{{}^0F_{-2}^1(\eta_\Sigma, 0)} \right\} \quad (7)$$

$$L_{total} = \frac{\sigma_L L_L + \sigma_\Sigma L_\Sigma}{\sigma_L + \sigma_\Sigma} \quad (8)$$

where L_L, L_Σ, and L_{total} are the Lorenz numbers for the L band, the Σ band, and both bands, respectively. Because of the low electrical conductivity, the carrier thermal conductivity is also low. With almost the same lattice thermal conductivity (the same lattice scattering), we achieved a total thermal conductivity lower than that of Na-doped PbTe.[20] The highest ZT value was ~1.3 at ~673 K for $K_{0.015}Pb_{0.985}Te$ (Figure 3), which is comparable with that of Na-doped PbTe at the same temperature.[20]

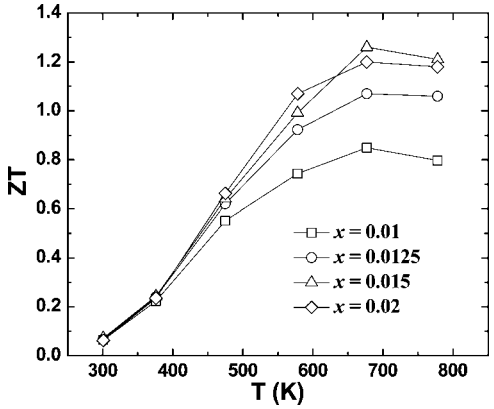

Figure 3. Temperature dependence of ZT for $K_xPb_{1-x}Te$ (x = 0.01, 0.0125, 0.015, and 0.02).

In both the PbTe and PbSe systems, K^+ and Na^+ dopants substitute for Pb^{2+}, and both K and Na have lower Pauling electronegativities (PE) than Pb (Table 2). In spite of their comparable ionic radii, the solubilities of K and Na are determined by the difference in the electronegativities of the average anion (Te^{2-} or Se^{2-}) and cation (Pb^{2+} together with K^+ or Na^+) after doping. Typically, a larger difference results in higher solubility. Since K has a lower electronegativity than Na, the average cation electronegativity after doping is lower in the case of K substitution. For PbTe, a lower average cation electronegativity reduces the electronegativity difference relative to the difference for Te^{2-} and Pb^{2+} without doping, so K has less solubility than Na in PbTe. For PbSe, the situation is opposite (a lower average cation electronegativity enlarges the electronegativity difference relative to Se^{2-} and Pb^{2+} without doping), so K has a higher solubility than Na in PbSe.

Samples of $K_xPb_{1-x}Se$ with different K concentrations (x = 0, 0.005, 0.010, 0.0125, and 0.015) were prepared and measured. The electrical conductivity, Seebeck coefficient, power factor, thermal diffusivity, specific heat, and thermal conductivity are shown in Figure 4a–f, respectively. It is clear that for $x \geq 0.01$, the electrical conductivity increased dramatically. The room-temperature Hall carrier concentration increased to $\sim 1.6 \times 10^{20}\ cm^{-3}$ (Figure 2, solid squares). Again we constructed the room-temperature Pisarenko plots for the single nonparabolic band model (dashed black line) and the two-band model (solid black line). For PbSe, we used $m_L^*/m_e = 0.28$ for the light-hole effective mass[23] and $m_\Sigma^*/m_e = 2.5$ for the heavy-hole effective mass, which was obtained from a first-principles calculation.[39] There was not much difference between the two models, suggesting that most of the contribution comes from the L band at room temperature, which agrees well with the previous

dx.doi.org/10.1021/ja301245b | J. Am. Chem. Soc. 2012, 134, 10031–10038

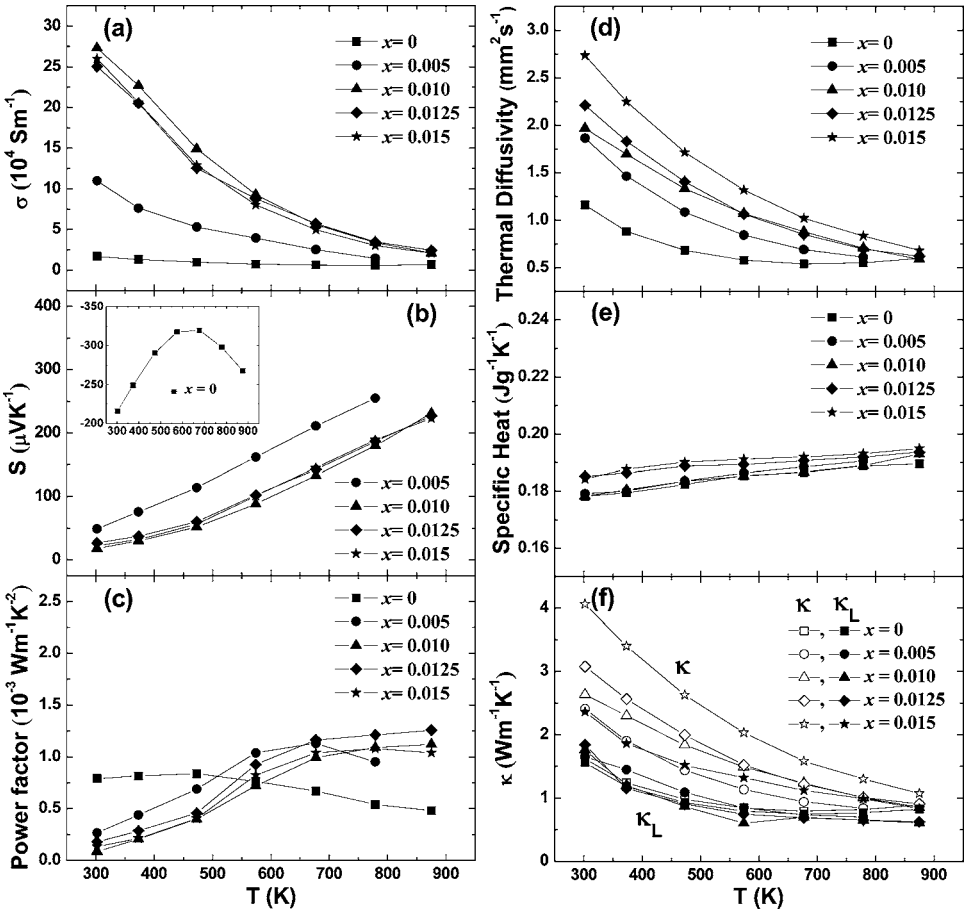

Figure 4. Temperature dependences of (a) electrical conductivity, (b) Seebeck coefficient, (c) power factor, (d) thermal diffusivity, (e) specific heat, and (f) total and lattice thermal conductivities for $K_xPb_{1-x}Se$ (x = 0, 0.005, 0.010, 0.0125, and 0.015).

results.[22] The pinning of the Fermi level by the heavy band happens only at high temperatures when the offset value of the two bands is small enough. A high Seebeck coefficient of ~210 μV K^{-1} at 875 K was obtained with the contribution from both bands. Since the band gap of PbSe increases with temperature (~0.43 eV at 850 K vs ~0.28 eV at 300 K), the Seebeck coefficient goes up all the way with increasing temperature without any sign of the bipolar effect. Low lattice thermal conductivities of ~1.7 W m^{-1} K^{-1} at 300 K and ~0.6 W m^{-1} K^{-1} at high temperature, similar to the previously reported values,[22] were calculated here for K-doped PbSe using L obtained from eqs 6−8. We noticed that the electrical conductivity decreased rapidly with increasing temperature, as indicated by the δ values shown in Table 1. However, with the high starting point of the electrical conductivity and the high Seebeck coefficient, the maximum ZT value reached was ~1.2 at 873 K (Figure 5), although the average ZT was clearly lower than that for K-doped $K_xPb_{1-x}Te$. Both the maximum ZT and the average ZT were comparable to those for Na-doped PbSe.

After studying K doping in PbTe and PbSe independently, we turned our attention to studying K doping in $PbTe_{1-y}Se_y$, with the aim of simultaneously increasing the power factor and further reducing the thermal conductivity to achieve higher ZT values. We fixed the K concentration in the Pb sites at 2% on the basis of the results for K in PbTe and PbSe, and we examined different Se concentrations in $K_{0.02}Pb_{0.98}Te_{1-y}Se_y$: y = 0.15, 0.25, 0.75, 0.85, and 0.95. All of the the XRD patterns (Figure 6) showed a single phase with the fcc rock salt

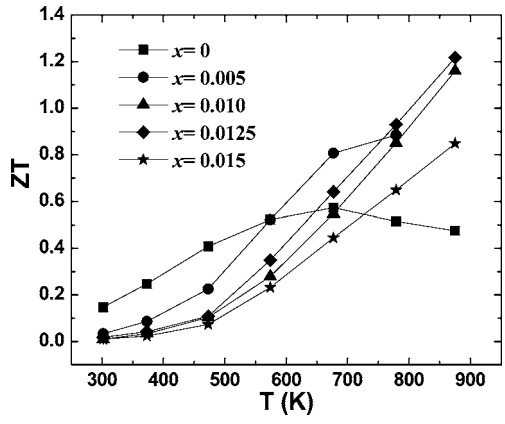

Figure 5. Temperature dependence of ZT for $K_xPb_{1-x}Se$ (x = 0, 0.005, 0.010, 0.0125, and 0.015).

structure. The peaks shifted to higher 2θ with increasing Se concentration because of the smaller lattice parameters. The good solid solution formation was confirmed by the good fit to Vegard's law (Figure 6 inset).

Figure 7 shows the room-temperature Hall carrier concentration as a function of (a) K and (b) Se concentration. With the help of Se, the Hall carrier concentration was effectively increased from $<6 \times 10^{19}$ cm^{-3} in PbTe to the optimized concentration of $(8-15) \times 10^{19}$ cm^{-3} for $PbTe_{1-y}Se_y$, consistent with the values observed in the previous reports.[20,22] The room-temperature Pisarenko plot for the

dx.doi.org/10.1021/ja301245b | J. Am. Chem. Soc. 2012, 134, 10031−10038

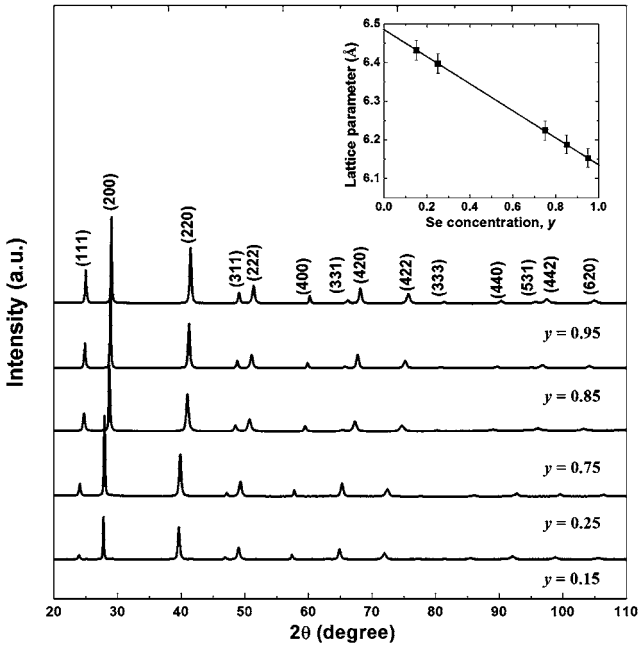

Figure 6. XRD patterns for $K_{0.02}Pb_{0.98}Te_{1-y}Se_y$ (y = 0.15, 0.25, 0.75, 0.85, and 0.95). The inset shows the lattice parameter relation with increasing Se concentration in $K_{0.02}Pb_{0.98}Te_{1-y}Se_y$.

$K_{0.02}Pb_{0.98}Te_{1-y}Se_y$ solid solution samples is shown in Figure 2 (solid triangles). The noticeable deviation of the Seebeck coefficient from the single-band model (dashed red line) for $K_{0.02}Pb_{0.98}Te_{1-y}Se_y$ (y = 0.15 and 0.25) supports the effects of heavy-hole bands. Because of the relatively low effective mass and larger energy difference between heavy-hole and light-hole band edges, ΔE, in PbSe, the Seebeck coefficients are lower than those of K-doped PbTe (solid circles). For $K_{0.02}Pb_{0.98}Te_{1-y}Se_y$ (y = 0.75, 0.85, and 0.95), more features come from K-doped PbSe. As the temperature increases, the two bands start to converge. We obtained good fits to the data using the energy differences between the conduction (C) band edge and the L and Σ band edges:

$$\Delta E_{C-L} = 0.18 + (4T/10000) - 0.04y$$
$$\Delta E_{C-\Sigma} = 0.42 + 0.10y \quad (9)$$

where y is the concentration of Se.[37,40] It has been concluded that the convergence of the electronic bands can provide more benefit for the enhancement of the Seebeck coefficient by multiple bands.[25] However, when y = 0 (PbTe), the L band will gradually move below the Σ band at a certain temperature and depart from the convergence. Thus, using Se to increase the convergence temperature (T_{cvg}) gives the most optimized Seebeck coefficient at high temperature (Figure 8 b). With

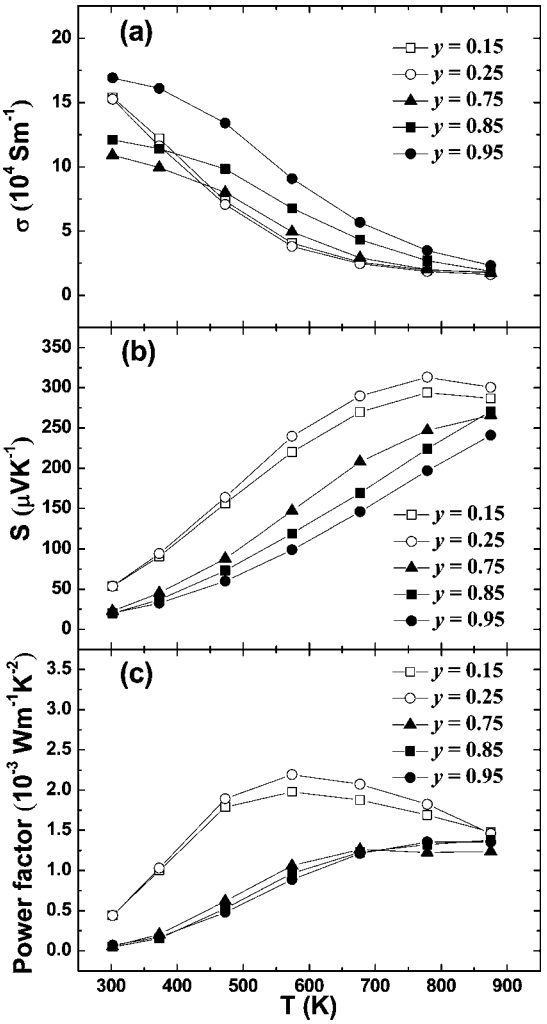

Figure 8. Temperature dependences of (a) electrical conductivity, (b) Seebeck coefficient, and (c) power factor for $K_{0.02}Pb_{0.98}Te_{1-y}Se_y$ (y = 0.15, 0.25, 0.75, 0.85, and 0.95).

increasing Se concentration, the temperature for the highest Seebeck coefficient increased. The highest Seebeck coefficient was ~320 μV K^{-1} at 775 K, which is much higher than the value of ~220 μV K^{-1} for Na-doped $PbTe_{1-y}Se_y$ at 775 K. The

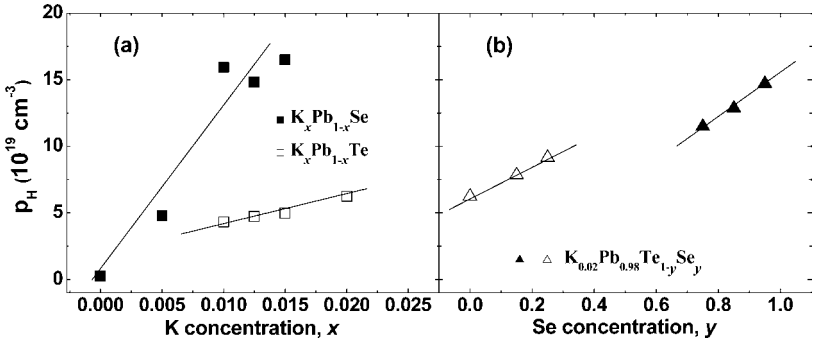

Figure 7. Hall carrier concentration at room temperature as a function of (a) K and (b) Se concentration.

dx.doi.org/10.1021/ja301245b | J. Am. Chem. Soc. 2012, 134, 10031−10038

successfully improved carrier concentration compensates for the loss in the carrier mobility resulting from the increased scattering of the electrons, which keeps the electrical conductivity the same at low temperature (Figure 8a). Fortunately, the decrease in the electrical conductivity is slowed with temperature, giving a smaller δ (Table 1). As a result, the power factor is enhanced at high temperature (Figure 8c).

The other obvious but very important role that Se plays is to decrease the lattice thermal conductivity by alloying scattering when it is used together with Te. The thermal diffusivity, specific heat, and total and lattice thermal conductivities for $K_{0.02}Pb_{0.98}Te_{1-y}Se_y$ (y = 0.15, 0.25, 0.75, 0.85, and 0.95) are shown in Figure 9a–c, respectively. The increased lattice

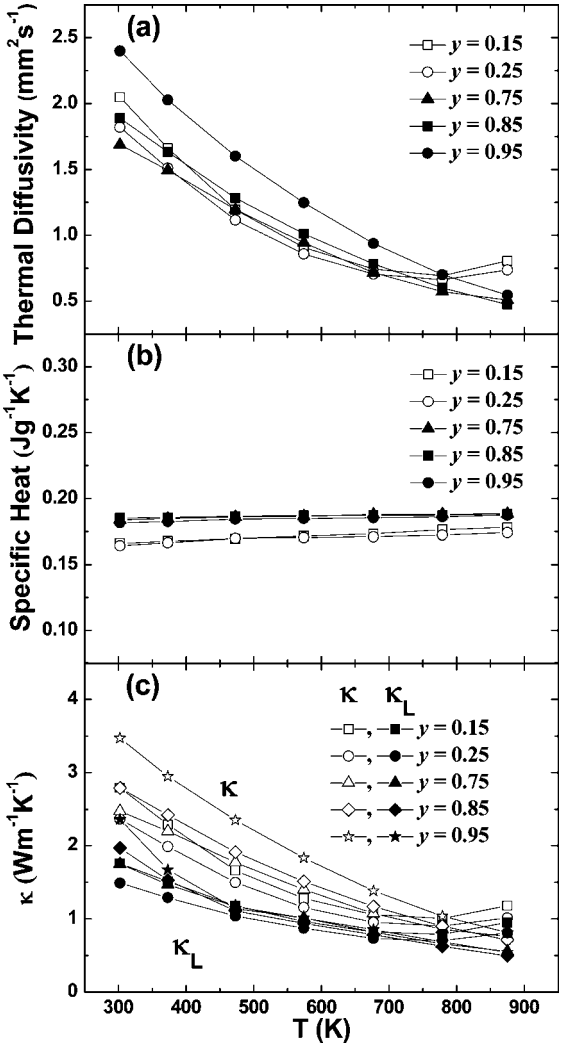

Figure 9. Temperature dependences of (a) thermal diffusivity, (b) specific heat, and (c) total and lattice thermal conductivities for $K_{0.02}Pb_{0.98}Te_{1-y}Se_y$ (y = 0.15, 0.25, 0.75, 0.85, and 0.95).

thermal conductivities at 800 K (Figure 9 c) may come from the error in the calculated values of L without considering the contribution from conduction band. It seems that increasing the Se concentration ($K_{0.02}Pb_{0.98}Te_{0.15}Se_{0.85}$) can increase the peak ZT to ~1.7 at ~873 K in comparison with the value of ~1.6 in $K_{0.02}Pb_{0.98}Te_{0.75}Se_{0.25}$ at ~773 K (Figure 10), but the Te-rich composition is clearly more promising for any applications below 873 K since the average ZT values are much higher.

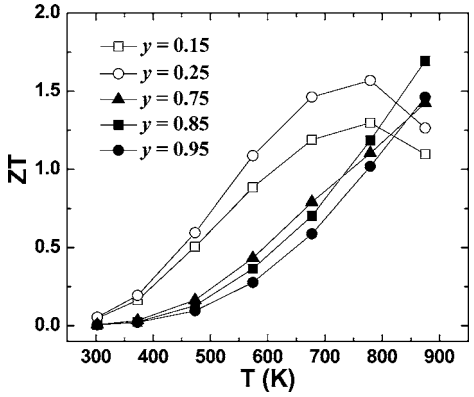

Figure 10. Temperature dependence of ZT for $K_{0.02}Pb_{0.98}Te_{1-y}Se_y$ (y = 0.15, 0.25, 0.75, 0.85, and 0.95).

Up to now, only Tl has been shown to induce resonant states in p-type PbTe, resulting in an extraordinary increase in the Seebeck coefficient.[18] However, with the help of a second valence band in PbTe, high ZT values can also be obtained by heavy doping with Na, K, and Mg, especially when combined with the alloy scattering introduced by PbSe or PbS.[20,25,26,41,42] Additionally, typical nanostructures have been created in the PbTe matrix to lower the lattice thermal conductivity by addition of a second phase and ball milling.[43,44] Other group IIIA elements (Al, Ga, and In),[45−47] group VIIA elements,[21] and some rare-earth elements[48] have proved to be good n-type dopants. A ZT value of >1.5 at 775 K was reached in La-doped PbTe with Ag_2Te nanoscale precipitates.[48] With decent ZTs in both p-type and n-type doping, PbTe is a promising candidate for thermoelectric applications in the near future.

CONCLUDING REMARKS

Potassium, an acceptor dopant in $K_xPb_{1-x}Te_{1-y}Se_y$, can strongly enhance the Seebeck coefficient by activating the heavy-hole band via heavy doping, which increases the DOS near the Fermi level. Combined with a lower lattice thermal conductivity due to increased point defects and the increased electrical conductivity at high temperature, higher peak ZT values of ~1.6 and ~1.7 were obtained in Te-rich samples $K_{0.02}Pb_{0.98}Te_{0.75}Se_{0.25}$ at 773 K and Se-rich samples $K_{0.02}Pb_{0.98}Te_{0.15}Se_{0.85}$ at 873 K, respectively, but the average ZT of the Te-rich samples was much higher than those of the Se-rich samples. Since Te is more expensive than Se, however, a trade-off between cost and performance needs to be considered for practical applications.

ASSOCIATED CONTENT

Supporting Information

Microstructures and chemical compositions for some samples; room-temperature Pisarenko plots for $K_xPb_{1-x}Te$ (x = 0.01, 0.0125, 0.015, and 0.02), $K_xPb_{1-x}Se$ (x = 0, 0.005, 0.010, 0.0125, and 0.015), and $K_{0.02}Pb_{0.98}Te_{1-y}Se_y$ (y = 0.15, 0.25, 0.75, 0.85, and 0.95) with the fitting line based on $\Delta E_{C-\Sigma}$ = 0.36 eV (see ref 40); and the relationship between carrier concentration and Hall carrier concentration for PbTe and PbSe. This material is available free of charge via the Internet at http://pubs.acs.org.

AUTHOR INFORMATION

Corresponding Author

gchen2@mit.edu; renzh@bc.edu

Notes

The authors declare no competing financial interest.

ACKNOWLEDGMENTS

This work was supported by "Solid State Solar-Thermal Energy Conversion Center (S^3TEC)", an Energy Frontier Research Center funded by the U.S. Department of Energy, Office of Science, Office of Basic Energy Sciences under Award DE-SC0001299 (G.C. and Z.R.), and National Science Foundation under grant No. 1066634 (D.B.).

REFERENCES

(1) Rowe, D. M. *CRC Handbook of Thermoelectrics*; CRC Press: Boca Raton, FL, 1995.

(2) Disalvo, F. J. *Science* **1999**, *285*, 703.

(3) Kraemer, D.; Poudel, B.; Feng, H. P.; Cavlor, J. C.; Yu, B.; Yan, X.; Ma, Y.; Wang, X. W.; Wang, D. Z.; Muto, A.; McEnaney, K.; Chiesa, M.; Ren, Z. F.; Chen, G. *Nat. Mater.* **2011**, *10*, 532.

(4) Harman, T. C.; Taylor, P. J.; Walsh, M. P.; LaForge, B. E. *Science* **2002**, *297*, 2229.

(5) Yan, X.; Joshi, G.; Liu, W. S.; Lan, Y. C.; Wang, H.; Lee, S.; Simonson, J. M.; Poon, S. J.; Tritt, T. M.; Chen, G.; Ren, Z. F. *Nano Lett.* **2011**, *11*, 556.

(6) Zhang, Q.; He, J.; Zhu, T. J.; Zhang, S. N.; Zhao, X. B.; Tritt, T. M. *Appl. Phys. Lett.* **2008**, *93*, No. 102109.

(7) Poudel, B.; Hao, Q.; Ma, Y.; Lan, Y. C.; Minnich, A.; Yu, B.; Yan, X.; Wang, D. Z.; Muto, A.; Vashaee, D.; Chen, X.; Liu, J.; Dresselhaus, D. S.; Chen, G.; Ren, Z. F. *Science* **2008**, *320*, 634.

(8) Sales, B. C.; Mandrus, D.; Williams, R. K. *Science* **1996**, *272*, 1325.

(9) Yu, C.; Zhu, T. J.; Zhang, S. N.; Zhao, X. B.; He, J.; Su, Z.; Tritt, T. M. *J. Appl. Phys.* **2008**, *104*, No. 013705.

(10) Kleinke, H. *Chem. Mater.* **2010**, *22*, 604.

(11) Dresselhaus, M. S.; Chen, G.; Tang, M. Y.; Yang, R. G.; Lee, H.; Wang, D. Z.; Ren, Z. F.; Fleurial, J. P.; Gogna, P. *Adv. Mater.* **2007**, *19*, 1043.

(12) Liu, W. S.; Yan, X.; Chen, G.; Ren, Z. F. *Nano Energy* **2012**, *1*, 42.

(13) Martin, J.; Wang, L.; Chen, L. D.; Nolas, G. S. *Phys. Rev. B* **2009**, *79*, No. 115311.

(14) Faleev, S. V.; Leonard, F. *Phys. Rev. B* **2008**, *77*, No. 214304.

(15) Zhang, Q.; Zhang, Q. Y.; Chen, S.; Liu, W. S.; Lukas, K.; Yan, X.; Wang, H. Z.; Wang, D. Z.; Opeil, C.; Chen, G.; Ren, Z. F. *Nano Energy* **2012**, *1*, 183.

(16) Scheele, M.; Oeschler, N.; Meier, K.; Kornowski, A.; Linke, C.; Weller, H. *Adv. Funct. Mater.* **2009**, *19*, 1.

(17) Zhang, Q.; Sun, T.; Cao, F.; Li, M.; Hong, M. H.; Yuan, J. K.; Yan, Q. Y.; Hng, H. H.; Wu, N. Q.; Liu, X. G. *Nanoscale* **2010**, *2*, 1256.

(18) Heremans, J. P.; Jovovic, V.; Toberer, E. S.; Samarat, A.; Kurosaki, K.; Charoenphakdee, A.; Yamanaka, S.; Snyder, G. J. *Science* **2008**, *321*, 554.

(19) Yu, B.; Zhang, Q. Y.; Wang, H.; Wang, X. W.; Wang, H. Z.; Wang, D. Z.; Snyder, G. J.; Chen, G.; Ren, Z. F. *J. Appl. Phys.* **2010**, *108*, No. 016104.

(20) Pei, Y.; LaLonde, A.; Iwanaga, S.; Snyder, G. J. *Energy Environ. Sci.* **2011**, *4*, 2085.

(21) LaLonde, A. D.; Pei, Y. Z.; Snyder, G. J. *Energy Environ. Sci.* **2011**, *4*, 2090.

(22) Wang, H.; Pei, Y.; LaLonde, A. D.; Snyder, G. J. *Adv. Mater.* **2011**, *23*, 1366.

(23) Zhang, Q. Y.; Wang, H.; Liu, W. S.; Wang, H. Z.; Yu, B.; Zhang, Q.; Tian, Z. T.; Ni, G.; Lee, S.; Esfarjani, K.; Chen, G.; Ren, Z. F. *Energy Environ. Sci.* **2012**, *5*, 5246.

(24) Androulakis, J.; Lee, Y.; Todorov, I.; Chung, D. Y.; Kanatzidis, M. *Phys. Rev. B* **2011**, *83*, No. 195209.

(25) Pei, Y.; Shi, X.; LaLonde, A.; Wang, H.; Chen, L.; Snyder, G. J. *Nature* **2011**, *473*, 66.

(26) Androulakis, J.; Todorov, I.; Chung, D.-Y.; Ballikaya, S.; Wang, G.; Uher, C.; Kanatzidis, M. *Phys. Rev. B* **2010**, *82*, No. 115209.

(27) Delaire, O.; Ma, J.; Marty, K.; May, A. F.; McGuire, M. A.; Du, M. H.; Singh, D. J.; Podlesnyak, A.; Ehlers, G.; Lumsden, M. D.; Sales, B. C. *Nat. Mater.* **2011**, *10*, 614.

(28) Ahmad, S.; Mahanti, S. D.; Hoang, K.; Kanatzidis, M. G. *Phys. Rev. B* **2006**, *74*, No. 155205.

(29) Xiong, K.; Lee, G.; Gupta, R. P.; Wang, W.; Gnade, B. E.; Cho, K. *J. Phys. D: Appl. Phys.* **2010**, *43*, No. 405403.

(30) Ahmad, S.; Hoang, K.; Mahanti, S. D. *Phys. Rev. Lett.* **2006**, *96*, No. 056403.

(31) Singh, D. J. *Phys. Rev. B* **2010**, *81*, No. 195217.

(32) Airapetyants, S. V.; Vinogradova, M. N.; Dubrovskaya, I. N.; Kolomoets, N. V.; Rudnik, I. M. *Sov. Phys. Solid State* **1966**, *8*, 1069.

(33) Khokhlov, D. *Lead Chalcogenides: Physics and Applications*; Taylor & Francis; New York, 2003.

(34) Allgaier, R. S. *J. Appl. Phys.* **1961**, *32*, 2185.

(35) Parker, D.; Singh, D. J. *Phys. Rev. B* **2010**, *82*, No. 035204.

(36) Noda, Y.; Orihashi, M.; Nishida, I. A. *Mater. Trans., JIM* **1998**, *39*, 602.

(37) Ravich, Y. I.; Efimova, B. A.; Smirnov, I. A. *Semiconducting Lead Chalcogenides*; Plenum Press: New York, 1970.

(38) Crocker, A. J.; Rogers, L. M. *Br. J. Appl. Phys.* **1967**, *18*, 563.

(39) Svane, A.; Christensen, N. E.; Cardona, M.; Chantis, A. N.; van Schilfgaarde, M.; Kotani, T. *Phys. Rev. B* **2010**, *81*, No. 245120.

(40) It should be noted that the gap between conduction and heavy-hole bands in PbTe is typically taken to be $\Delta E_{C-\Sigma} = 0.36$ eV. As shown in the Supporting Information, we found a poorer fit to the data using this value of $\Delta E_{C-\Sigma}$ in comparison with the value of 0.42 eV given in eq 9.

(41) Jaworski, C. M.; Wiendlocha, B.; Jovovic, V.; Heremans, J. P. *Energy Environ. Sci.* **2011**, *4*, 4155.

(42) Pei, Y. Z.; LaLonde, A. D.; Heinz, N. A.; Shi, X. Y.; Lwanaga, S.; Wang, H.; Chen, L. D.; Snyder, G. J. *Adv. Mater.* **2011**, *23*, 5674.

(43) Biswas, K.; He, J. Q.; Zhang, Q. C.; Wang, G. Y.; Uher, C.; Dravid, V. P.; Kanatzidis, M. G. *Nat. Chem.* **2011**, *3*, 160.

(44) Zhang, Q. Y.; Wang, H. Z.; Zhang, Q.; Liu, W. S.; Yu, B; Wang, H.; Wang, D. Z.; Ni, G.; Chen, G.; Ren, Z. F. *Nano Lett.* **2012**, *12*, 2324.

(45) Jaworski, C. M.; Heremans, J. P. *Phys. Rev. B* **2012**, *85*, No. 033204.

(46) Volkov, B. A.; Ryabova, L. I.; Khokhlov, D. R. *Phys. Usp.* **2002**, *45*, 819.

(47) Jovovic, V.; Thiagarajan, S. J.; Heremans, J. P.; Komissarova, T.; Khokhlov, D.; Nicorici, A. *J. Appl. Phys.* **2008**, *103*, No. 053710.

(48) Pei, Y. Z.; Lensch-Falk, J.; Toberer, E. S.; Medlin, D. L.; Snyder, G. J. *Adv. Funct. Mater.* **2011**, *21*, 241.